One-step formation of TiO_2 hollow spheres via a facile microwave-assisted process for photocatalytic activity

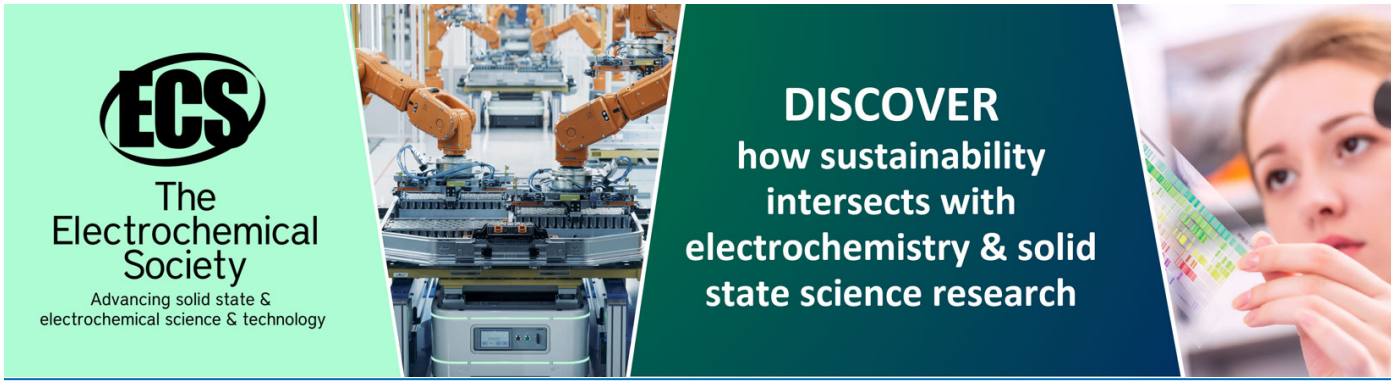

IOP Publishing Nanotechnology
Nanotechnology 29 (2018) 145707 (9pp) https://doi.org/10.1088/1361-6528/aaabee

One-step formation of TiO_2 hollow spheres via a facile microwave-assisted process for photocatalytic activity

Firas K Mohamad Alosfur[1,4], Noor J Ridha[2], Mohammad Hafizuddin Haji Jumali[3,4] and S Radiman[3]

[1] Department of Physics, College of Science, University of Kerbala, 56001 Karbala, Iraq
[2] Department of Chemistry, College of Science, University of Kerbala, 56001 Karbala, Iraq
[3] School of Applied Physics, Faculty Science and Technology, Universiti Kebangsaan Malaysia, 43600 Bangi, Selangor, Malaysia

E-mail: frsos2005@yahoo.com and hafizhj@ukm.edu.my

Received 6 December 2017, revised 23 January 2018
Accepted for publication 31 January 2018
Published 19 February 2018

Abstract

Mesoporous TiO_2 hollow spherical nanostructures with high surface areas were successfully prepared using a microwave method. The prepared hollow spheres had a size range between 200 and 500 nm. The spheres consisted of numerous smaller TiO_2 nanoparticles with an average diameter of 8 nm. The particles had an essentially mesoporous structure, with a pore size in the range of 2–50 nm. The results confirmed that the synthesised of anatase TiO_2 nanoparticles with specific surface area approximately 172.3 $m^2 g^{-1}$. The effect of ultraviolet and visible light irradiation and catalyst dosage on the TiO_2 photocatalytic activity was studied by measuring the degradation rate of methylene blue. The maximum dye degradation performances with low catalyst loading (30 mg) were 99% and 63.4% using the same duration of ultraviolet and visible light irradiation, respectively (120 min).

Keywords: TiO_2 hollow spheres, microwave, mesoporous, photocatalysis

(Some figures may appear in colour only in the online journal)

1. Introduction

In the past few decades, the amount of waste generated by human activities has increased tremendously. In the same period, the demand for clean water for human consumption, agriculture and industry has rapidly increased [1]. Due to limited resources for clean water, the removal from effluent of contaminants such as dyes in textile wastewater is becoming a pressing need [2, 3]. Various methods have been developed for the removal of dyes from effluents, including physical methods such as precipitation [4, 5], adsorption [6] and reverse osmosis [7]; chemical methods via oxidation and reduction [8]; and biological methods including aerobic and anaerobic treatment [9, 10]. Unfortunately, these methods often have several shortcomings, such as creation of sludge, high operating costs, time consumption, low yield and inefficiency, especially in cases where complicated aromatic compounds are produced.

In recent years, decomposing compounds using photocatalytic processes by semiconductor degradation methods have received greater attention [11–13]. Unlike the methods mentioned above, photocatalytic degradation is well accepted as a cleaner and greener technology for the elimination of toxic organic and inorganic pollutants from water and wastewater. Moreover, this method is economical, since it requires little energy to operate, and works at ambient temperature and pressure [14, 15]. Since the first report on its photocatalytic activity [16], TiO_2 has attracted huge interest from researchers for many decades as the best semiconductor for the photodegradation of organic pollutants in water. TiO_2 exhibits chemical stability, high oxidation resistance, low toxicity, long-term photostability and competitive production cost [17, 18].

The photocatalytic activity of TiO_2 is highly dependent on its surface area, crystalline structure and synthesis method

[4] Authors to whom any correspondence should be addressed.

[19, 20]. Various methods have been studied to enhance the photocatalytic performance via increasing the surface area of TiO_2 [21, 22], generating defects to motivate space-charge separation [23] and doping TiO_2 with other semiconductors or metals [24, 25]. Among these methods, the easiest and most effective approach to enhancing photocatalytic efficiency is increasing the TiO_2 surface area. TiO_2 with a high surface area is a highly active photocatalyst material, due to its high surface-to-volume ratio, which absorbs light and provides additional active sites for catalytic reactions [26, 27].

Having large specific surface area, TiO_2 hollow spheres display interesting optical and electrical properties. There are several reports on their improved light-harvesting capacity, enhanced penetration, low density and smaller band gap—which leads to a wider wavelength absorption region [28, 29]. Thus, it is not surprising that TiO_2 hollow spheres are being suggested as one of the promising nanostructures for efficient sunlight photocatalyst applications.

TiO_2 hollow spheres can be prepared using various methods [30–32]. However, the conventional methods usually require high pressures and temperatures, involve long reaction times, and utilise complex procedures. In addition, localized overheating output from the hot surface of the reaction vessel can lead to product decomposition in case of heating for elongated periods. Unlike these conventional preparation methods, where the heat is transferred by conductance, the microwave method produces potential and uniform internal heating by the direct coupling of microwave energy with the polar molecules present in the reaction mixture [33, 34]. Microwave dielectric heating is introduced into the vessel reactor remotely, depending on the ability of the solvent or matrix to absorb the microwave energy by, and thus convert it into heat. The solvent absorbs the microwave irradiation by two mechanisms: dipole polarisation and conduction.

Here, we present a simple, high yield, efficient reaction to prepare mesoporous TiO_2 hollow spheres with high surface area, using a novel modified microwave method which works much faster than conventional methods. A possible mechanism of TiO_2 hollow sphere formation has also been proposed. The effect of different loading amounts of TiO_2 nanoparticles on the photocatalytic activity has been studied via the photodegradation of MB ($C_{16}H_{18}N_3SCl \cdot 3H_2O$) dye in aqueous solution under both ultraviolet and visible light irradiation.

2. Experimental procedure

2.1. Synthesis of TiO_2 hollow spheres

The TiO_2 hollow spheres were prepared using a modified commercial domestic microwave oven (Sharp model R-369T) complete with a reflux device and magnetic stirrer. The modified microwave process consisted of drilling a 35 mm hole on the top side of the microwave to provide space for a reflux condenser to facilitate work at ambient pressures. Titanium (IV) isopropoxide (TTIP, $Ti[OCH(CH_3)_2]_4$, bought from Acros Organics, 98%) was used as the precursor. In a typical procedure, 0.2 M of TTIP was added dropwise into a glass vessel containing ethanol (pH = 2) under vigorous stirring for 10 min at room temperature. Next, 100 ml of ethanol was added to the solution to slow the hydrolysis and condensation reactions, after which 5 ml of deionised water was added dropwise to the mixture with continuous vigorous stirring for 3 h. The solution was then placed in the microwave for 5 min at 50% of the maximum microwave power (1100 W). The solution changed from transparent to milky white, indicating that TiO_2 nanoparticles were produced directly by exposure to microwave radiation. Next, the precipitate was centrifuged at 4000 rpm for 5 min and repeatedly washed with absolute ethanol and distilled water to eliminate any residual organic species remaining in the final products. The precipitate was then dried at 90 °C in air overnight. Finally, the white fine powder was calcined at 500 °C in air for 1 h to obtain TiO_2 nanoparticles.

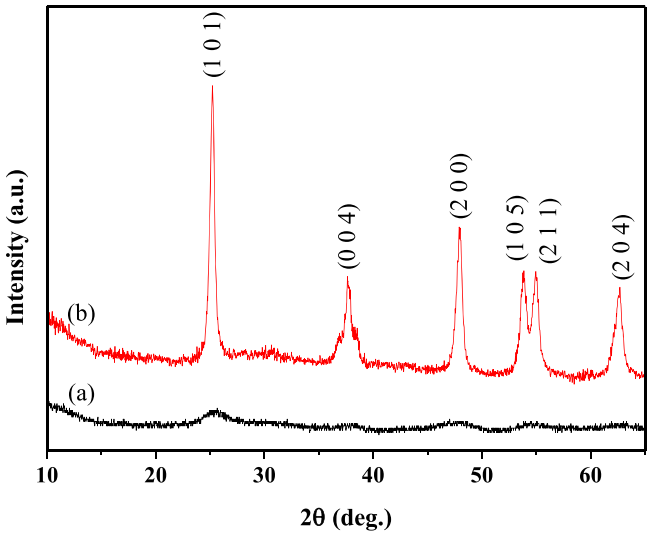

Figure 1. XRD patterns of the as-prepared TiO_2 (a) and TiO_2 calcined at 500 °C in air for 1 h (b).

2.2. Characterisation

2.2.1. X-ray diffraction analysis. The phase identification of the powder was conducted at room temperature by XRD (Bruker D8 Advance) using Cu Kα radiation operating at 40 kV and 40 mA. The 2θ range was from 10° to 65° with a step size of 0.025° and an exposure time of 19 s per step. The crystallite size of the prepared powder was calculated using TOPAS V4 software (Bruker Diffract-Plus).

2.2.2. Field-emission scanning electron microscopy (FE-SEM). The sample morphology was investigated using FE-SEM (SUPRA 55VP, ZEISS) operated at accelerating voltages of 3 to 30 kV. The powder was mounted on a conductive carbon tape prior to the measurement.

2.2.3. BET surface area measurements. The surface area of the powder was analysed using a Gemini apparatus (Micromeritics 2010 Instrument Corporation). The

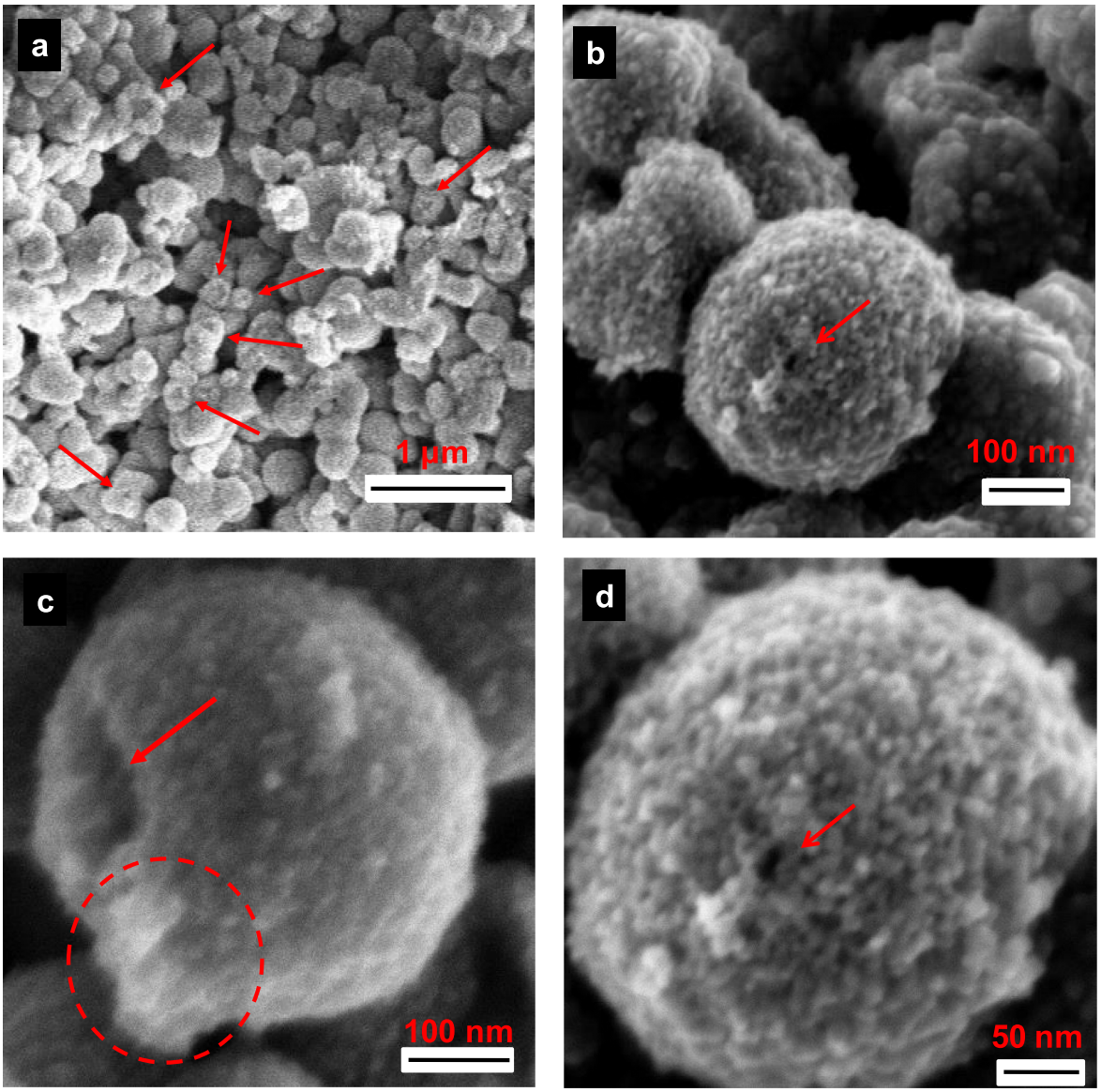

Figure 2. FE-SEM images of TiO_2 nanoparticles at different magnification: 10 k (a), 50 k (b), 100 k (c) and 160 k (d). Arrows correspond to the presence of hollow spheres while the red circle marked to the cracked part.

measurements were based on N_2 (>99.999%) adsorption isotherms at 77.35 K using the Brunauer–Emmett–Teller (BET) process at 350 °C for 2 h under 50 mTorr of vacuum. The pore volume and average pore size distribution were obtained via the Barrett–Joyner–Halenda (BJH) technique from the nitrogen desorption isotherm.

2.2.4. X-ray photoelectron spectroscopy (XPS). The surface state of the powder was examined using extremely high-vacuum XPS (AXIS ULTRA DLD). The x-ray source used in this work was Mg Kα operating at 10 mA and 15 kV. The pressure in the measuring chamber was fixed at 10^{-9} torr. The survey scan was conducted using pass energy set at 160 eV, and the high-resolution spectra for all elements were collected using 20 eV. The data were baseline-corrected and analysed using Vision processing software. The instrumentation transmission function was corrected using Schofield sensitivity factors. The charging effects of binding energies (BEs) were decreased by applying a flood gun at low kinetic energy. The binding energies were calibrated based on the graphite C 1s peak at 284.5 eV. The corrected BEs were used to identify the valence and chemical environment of the atom studied.

2.3. Photocatalytic activity test. The photocatalytic activity of the synthesised TiO_2 nanoparticle was evaluated by monitoring the degradation of methylene blue (MB) solution as the target pollutant in aqueous solution. Methylene blue was selected due to its high adsorption to metal oxide surfaces, well defined optical absorption and good resistance to light degradation. The experiment was conducted at room temperature with an initial pH of 7.0. The effect of catalyst dosage was studied as a function of irradiation time. Two types of light were used to study the

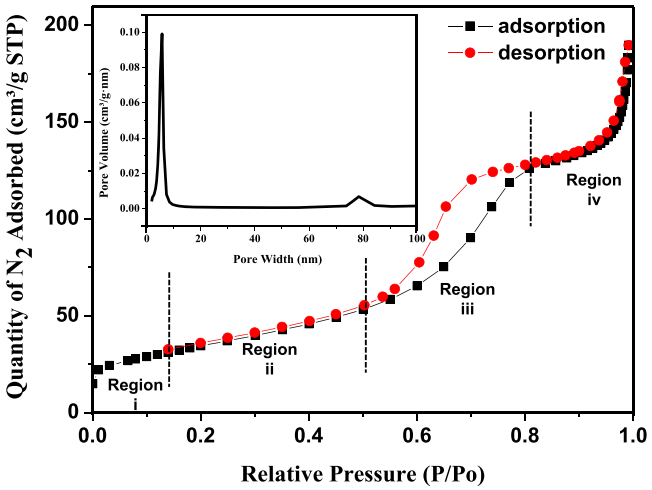

Figure 3. N_2 adsorption–desorption isotherm and pore diameter distribution (inset) of anatase TiO_2 nanoparticles.

effect of the irradiation source on the dye degradation: a 20 W commercial halogen tungsten lamp was used as the visible light (VL) source and a 12 W VL-6.LC lamp at 365 nm was used as the UV source. In each experiment, a given amount of catalyst (10, 20, 30, 40 or 50 mg) was suspended in 100 ml of aqueous MB (10 mg L^{-1}) in a 250 ml conical flask. Prior to irradiation, the solution was sonicated for 10 min and preserved in a dark room for at least 1 h to ensure adsorption−desorption homogeneity of the dye on the catalyst surface. The first sample (approximately 5 ml) was taken at the end of the period for the dark adsorption (just before the light was switched on) to determine the MB concentration in the solution, which was considered the elementary concentration (c_0). The flask was then continuously mechanically shaken at 400 rpm under irradiation by a light source located axially to the container at a distance of 20 cm. After specific intervals, approximately 5 ml of the liquid was withdrawn regularly and promptly centrifuged to remove any suspended solid. To monitor the MB degradation, the clean solution was analysed using UV −visible spectrometry (Perkin Elmer Lambda 900 UV/Vis) in the range 450–750 nm.

3. Results and discussion

3.1. X-ray diffraction analysis

Figure 1 shows the x-ray diffractograms of the prepared TiO_2 nanoparticles (before and after calcination). The as-synthesised TiO_2 nanoparticles (uncalcined) show broad and weak peaks, due to the small average crystallite size and poor crystallisation (figure 1(a)). Crystalline peaks were observed after calcination (figure 1(b)). Sharp peaks with high intensities identified as the anatase phase (JCPDS # 021-1272) for the calcined TiO_2 confirmed the formation of highly crystalline material. The average crystallite size was determined

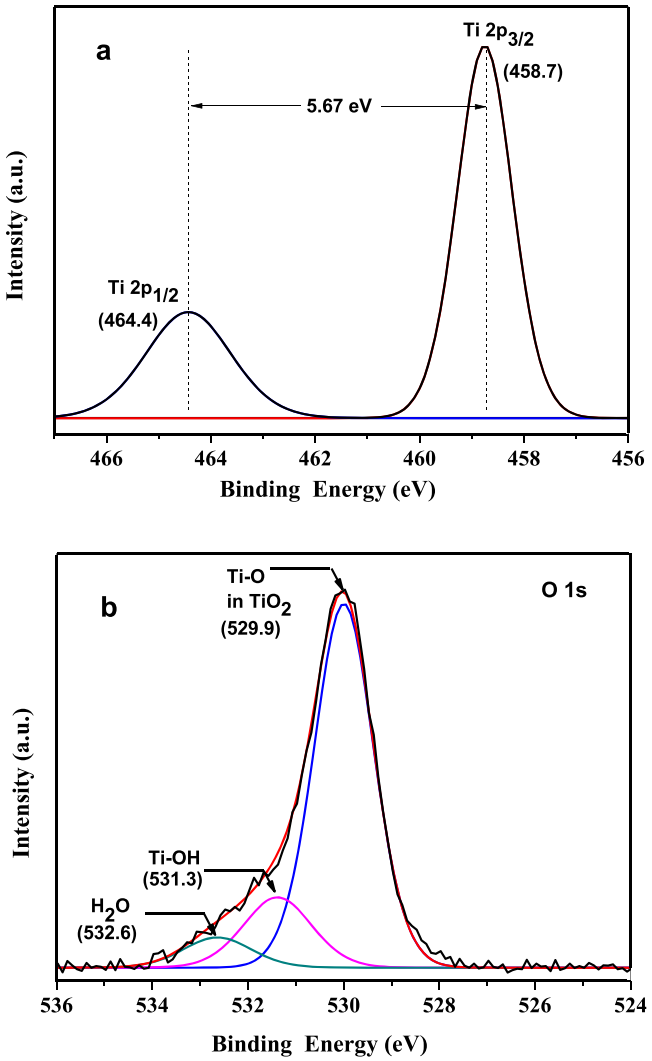

Figure 4. XPS spectra of Ti 2p (a) and O1s (b) from TiO_2 nanoparticles.

using TOPAS V4 software as approximately 4.5 nm and 11.9 nm before and after calcination, respectively.

3.2. Surface morphology

The morphology and structure of TiO_2 nanoparticles were examined by FE-SEM. The low-magnification in figure 2(a) revealed that the TiO_2 nanoparticles mainly possessed spherical shape with rough surfaces. The average diameter of these spheres was approximately 500 nm. Moreover, we can also observe that the spherical particles have a hollow inner cavity with thick wall. The hollow spheres are indicated by red arrows. The high magnification (figures 2(b)–(d)) show that these spheres are composed of numerous smaller TiO_2 nanoparticles with an average diameter of 8 nm. A small amount of aggregated nanoparticles can be observed maybe existing from precursors or cracked hollow spheres. The cracked part marked with the red circle as shown in figure 2(c).

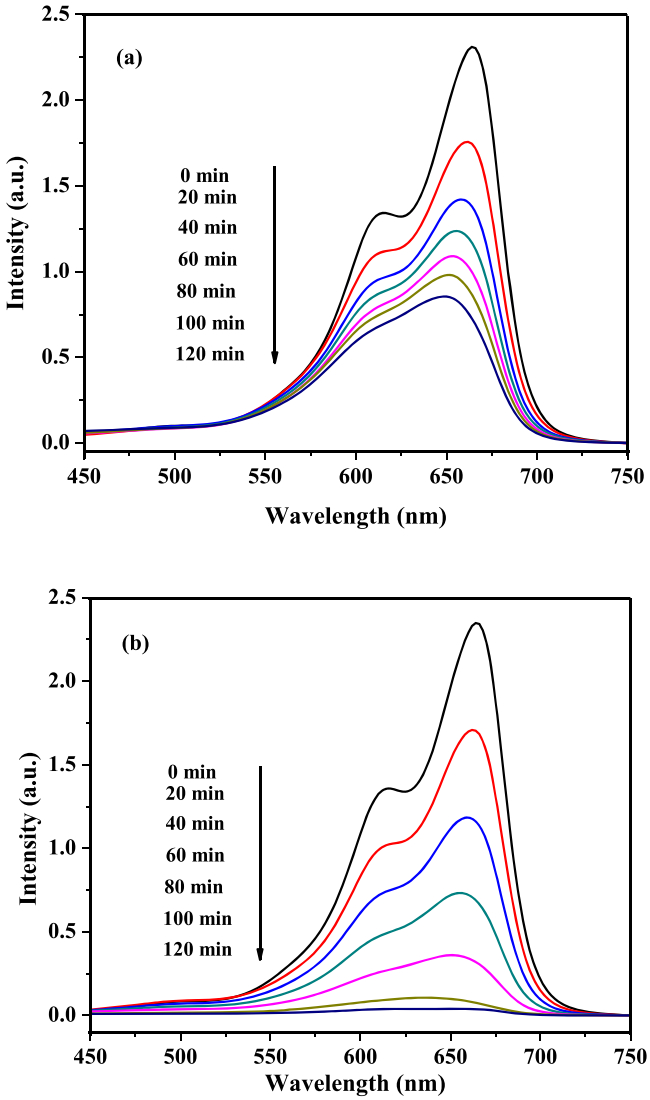

Figure 5. UV–vis absorption spectra of MB solution after photocatalysis by 30 mg of TiO_2 with different illumination times under UV (a) and VL (b) irradiation.

The nanospheres' structure was further identified by the TEM image as shown in figure 3. The nanospheres' surfaces consist of plentiful agglomerated TiO_2 nanoparticles with diameter around 7 nm, and a significant amount of mesopores with diameters of 3–6 nm are displayed. These nanoparticles' agglomeration may be due to insufficient reaction time inside the microwave. The black area noted in the figures may be due to the inner cavity of the hollow spheres.

3.3. Specific surface area and pore distributions

Figure 3 shows the typical N_2 adsorption and desorption of anatase TiO_2 nanoparticles. According to BDDT classification, the isotherms can be classified into four different regions:

(i) At low relative pressures (below 0.2), the isotherm displays gradual increment of adsorption, suggesting that the powders have micropores (type I).

(ii) At intermediate relative pressure (corresponding to pressure between 0.2 and 0.5), feeble hysteresis loops are observed, and can be attributed to type H2, indicating the powder contains mesopores with narrow necks and wider bodies (ink-bottle pores) [35].

(iii) Step in the P/P0 range of 0.5–0.8 corresponding to isotherm with type IV, which reveals distinct capillary condensation [36]. In addition, a hysteresis loop is clearly observed and attributed to type H2; such a loop is often associated with pores with narrow necks and wider bodies (ink-bottle pores) [37]. This observation confirms the hollow spherical structure of nanoparticles in the sample.

(iv) At high relative pressures above 0.8, a small hysteresis loop can be identified, indicating the presence of larger mesopores (type IV) [38–41].

On the other hand, the sharp decline in the desorption curve also confirms the presence of mesoporosity (2–50 nm) in the material [42]; the mesoporous structure of TiO_2 nanoparticles can be ascribed to formation of pores between TiO_2 particles [43, 44]. Such mesoporous structure can improve the rate of photocatalytic reactions [45].

The specific surface area of the TiO_2 nanoparticles was found to be approximately 172.3 $m^2\,g^{-1}$. The surface area of the synthesised sample in this work was greater than the that of TiO_2 nanospheres reported in the literature, which ranged between 102.9 $m^2\,g^{-1}$ [46], 123 $m^2\,g^{-1}$ [47] and 57.0 $m^2\,g^{-1}$ [48]. Generally, large surface area is possible to exhibit better photocatalytic activity, because a large surface area provides more active sites to adsorb methylene blue solution [49].

The pore size distribution of TiO_2 nanoparticles is shown in the inset of figure 3; it can be seen that the spherical TiO_2 nanoparticles reveal bimodal pore size distributions with small and large pore sizes. The average pore diameter of small pores is distributed around approximately 5 nm, while that of the large pores has peak pore diameters about 78 nm. Therefore, the average pore size distribution also confirms the mesoporous nature of the sample.

Ggenerally, there is a relationship between average pore size and the crystallite size of TiO_2 nanoparticles, where the average pore size increased with an increase in the crystallite size of TiO_2 powders [50–53]. This bimodal mesopore size distribution corresponds to the two different aggregates in the powders. The first is attributed to the small intra-aggregated mesopores created between intra-agglomerated main particles (represented the hysteresis loop at the lower P/P0 range), and probably consists of voids that are left between agglomerations of nanoparticles in the TiO_2 shell. The second is attributed to aggregates in the powders corresponding to the large interaggregated mesopores produced by interaggregated secondary particles (hysteresis loop at the higher P/P0 range), and corresponds to the pores inside the hollow spheres.

3.4. X-ray photoelectron spectroscopy (XPS)

The narrow scan of XPS spectra for Ti and O taken on the surface of TiO_2 is shown in figure 4. The photoelectron peak

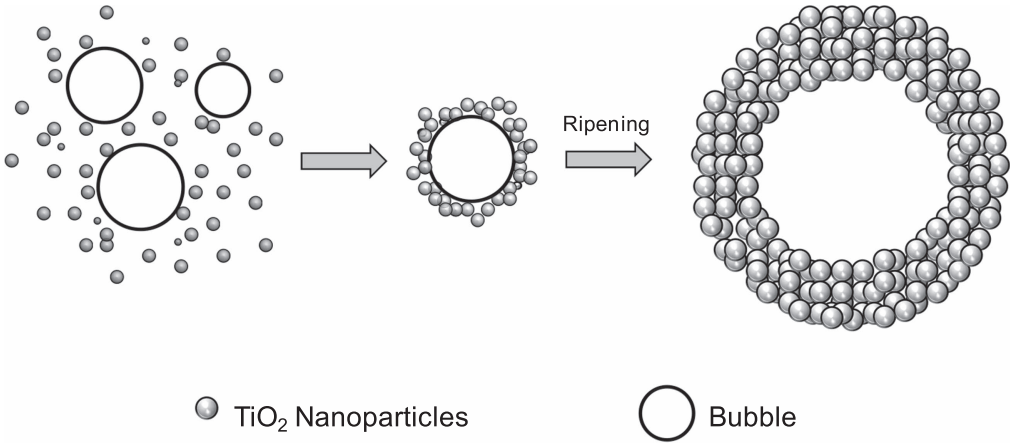

Scheme 1. Schematic growth mechanism of the TiO_2 hollow spheres via Ostwald ripening.

of Ti 2p region was resolved as depicted in figure 4(a). The peaks positioned at binding energies of 458.7 and 464.4 eV were attributed to Ti $2p_{3/2}$ and Ti $2p_{1/2}$ spin−orbital splitting in the Ti^{4+} chemical state, respectively. In addition, the splitting between these two peaks was found to be 5.67 eV, which is in good agreement with the literature values [54]. This value clearly indicates the presence of Ti^{4+}, and is consistent with the presence of anatase TiO_2 [55].

3.5. Growth mechanisim

Based on the experimental results and analysis, the TiO_2 nanoparticle was obtained by hydrolysis starting from titanium isopropoxide. In acidified ethanol solution, the reaction takes place into two steps—hydrolysis of titanium isopropoxide (equation (1)) is followed by condensation (equation (2)):

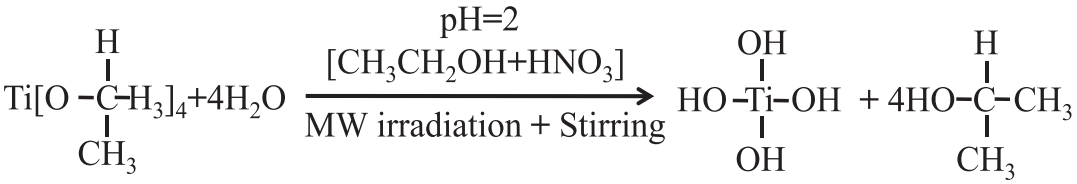

(1)

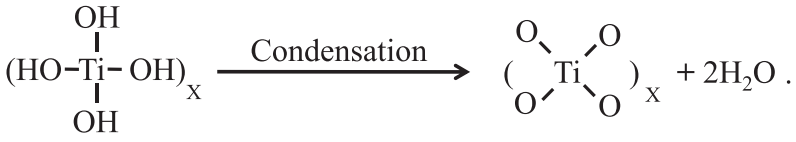

(2)

The O 1s peak can be deconvoluted into three contributions at 529.9, 531.3 and 532.6 eV. The main peak (529.9 eV) was assigned to Ti–O in TiO_2. The other peaks can be attributed to hydroxyl groups from either Ti–OH or adsorbed H_2O. The existence of hydroxyl can be attributed to the fact that TiO_2 can easily adsorb water vapor in air, leading to hydroxyl formation on the surface. Du *et al* (2008) argued that the formation of catalysts such as TiO_2 with large amount of surface hydroxyl groups play an important role in enhancing the photocatalytic activity, where this quantity is proportional to the surface area of the catalysts. Based on these results, high-purity TiO_2 nanoparticles were successfully synthesised using microwave irradiation.

The acid condition and the increase in alcohol concentration provide control to the avoiding TiO_2 precipitation by slow down the hydrolysis reaction. Therefore, several factors should be included for obtaining a desired shape and size of the TiO_2 nanoparticles. Among these factors are the time and temperature of the reaction, the amount and concentration of each of TiO_2 precursor, acids, alcohols and deionized water.

The possible formation mechanism of TiO_2 hollow spheres can be suggested depending on the reaction system, as shown in scheme 1. At first, fine TiO_2 nanoparticles are formed. Meanwhile, isopropyl alcohol (C_3H_8O) decomposes under heating to produce some gas bubbles. These bubbles

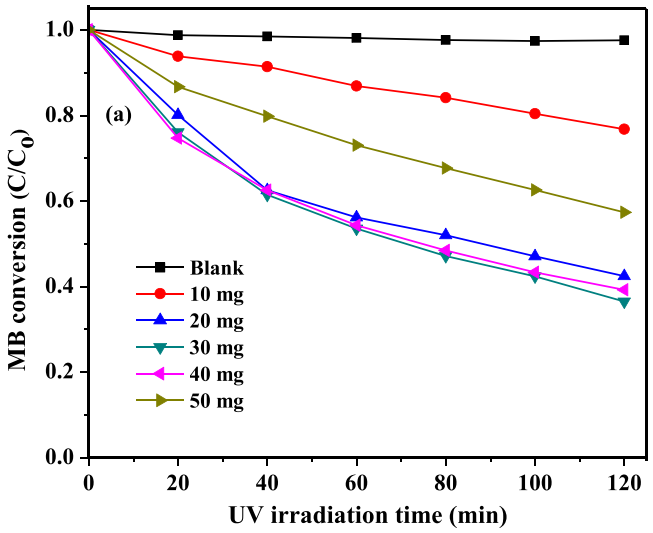

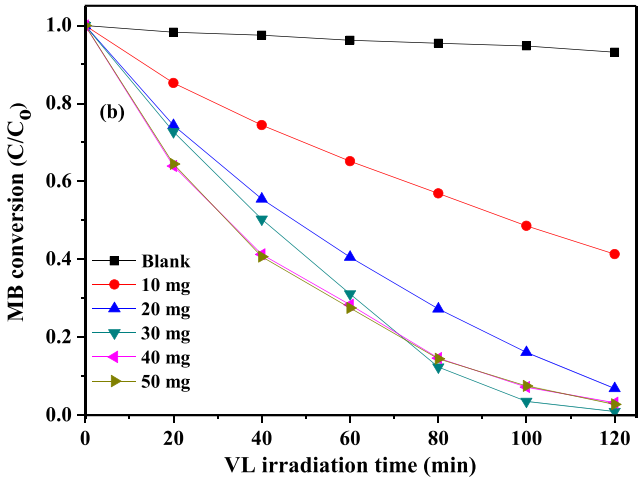

Figure 6. Effect of TiO_2 nanoparticle dosage on photocatalytic MB degradation versus irradiation time under UV (a) and VL (b) irradiation.

can act as templates for the formation of hollow spheres, where TiO_2 nanoparticles tend to aggregate on the gas bubble surfaces to reduce the interfacial energy, thereby forming the spherical aggregates. It is known that many factors can affect the attachment of particles on the gas bubble surfaces, such as particle size, surface properties, electrostatic interactions and hydrodynamic conditions. With increased reaction time, migration of TiO_2 nanoparticles will sustainably reach a certain level, after which the hollow sphere structure will be obtained after escape of bubbles from the core. This phenomenon can be attributed to the Oswald ripening process during heating [56], where continual aggregation of TiO_2 occurs on the bubble surface. Finally, the mesoporous TiO_2 hollow spheres are created. Thus, isopropyl alcohol plays an essential role in the formation of mesoporous hollow TiO_2 spheres.

3.6. Photocatalytic activity

Figure 5 shows the changes in the maximum absorption spectra of MB for 664 nm irradiation in the presence of 30 mg

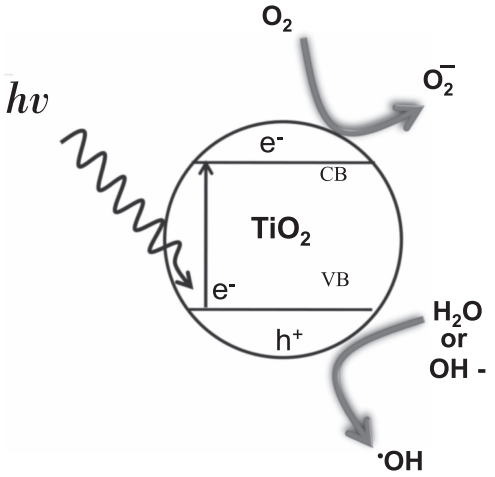

Figure 7. The proposed mechanism of photocatalysis by TiO_2 nanoparticles.

of TiO_2 under UV and VL irradiation. As the irradiation time was increased, the intensities of the maximum absorption peaks decreased. The peaks became very weak and nearly disappeared after 120 min of irradiation with VL, which indicates almost complete degradation of MB. The absorption peaks were slightly blue shifted during the course of the photodegradation, due to the small crystal size of the TiO_2 [57]. This shift indicates an increase in the reduction potential and oxidising potential for electrons and holes respectively. The electrons and holes with high reduction and oxidation power, respectively, enhanced the photodegradation rate.

The residual concentration ratios c/c_0 of MB (at 664 nm) *versus* degradation time (t) are shown in figure 6. Essentially, the degradation ratio increases with increasing catalyst dosage, and then decreases after a specific catalyst dosage. All of the TiO_2 samples exhibited increased MB degradation under VL irradiation than under UV irradiation. The blank run (without TiO_2) showed that the degradation can be ignored, as the MB could not be decomposed under light irradiation without the photocatalyst. Among the TiO_2 catalyst dosages studied, the 30 mg dosage offered the best efficiency for MB degradation under both UV and VL irradiation. This is due to fact that an increased opacity of the suspension brought about by the excess TiO_2 particles, which decrease the light penetration. The maximum performance of MB removal with catalyst loading (30 mg) for a given time period reached 99% and 63.4% under VL and UV irradiation, respectively, after 120 min—indicating that the TiO_2 prepared herein had high photocatalytic activity. The VL response can be attributed to the high surface area of the nanocatalyst, where TiO_2 hollow sphere structure allows more efficient use of the light source, and thereby offers improved catalytic activity [58–61]. In addition, the organization of TiO_2 nanoparticles into a hierarchical structure can prevent the nanoparticles from randomly aggregating, so that high catalytic efficiency can be maintained.

The steps of photocatalytic reactions occurring on the TiO_2 surface can be proposed as shown in figure 7. When TiO_2 is illuminated by a photon with energy equal or higher

than its band gap, electrons (e^-) will jump from the valence band (VB) to the conduction band (CB). This process produces a positive charge in VB termed a hole (h+) and a free electron (e^-) in the CB. Generally, the adsorbed H_2O or hydroxide ions (OH^-) on the TiO_2 surface can react with hole in the VB to generate hydroxyl radicals (•OH), while the electron in the CB can reduce O_2 in the surroundings to produce superoxide ions (O_2^-). The most important reaction of MB photodegradation involves turning hydroxyl ions (OH^-) into hydroxyl radicals (•OH) by reaction with the holes on the TiO_2 surface [62].

4. Conclusions

TiO_2 hollow spheres with high photocatalytic activity for MB degradation were successfully synthesised using a modified microwave method. The sample characteristics showed that the prepared TiO_2 nanoparticles had a small particle size (average 15 nm), a pure anatase phase and a high surface area with a mesoporous structure. The small amount of TiO_2 nanocatalyst obtained has a strong effect on MB degradation under visible light irradiation. This study suggests that this modified microwave synthesis technique for TiO_2 nanoparticles has good economic potential for removing pollutants, and deserves further study.

Acknowledgments

This work was supported by the Universiti Kebangsaan Malaysia (UKM) through grant no. UKM-AP-2015-006, as well as grant nos. GUP-2014-012 and DIP-2016-027. The authors are grateful to Mr Mohamad Hasnul Naim for his assistance with the FE-SEM measurements.

ORCID iDs

Firas K Mohamad Alosfur https://orcid.org/0000-0001-5023-9384

References

[1] Jiang G, Zheng X, Wang Y, Li T and Sun X 2011 Photodegradation of methylene blue by multi-walled carbon nanotubes/TiO_2 composites *Powder Technol.* **207** 465–9
[2] Le H A, Linh L T, Jurng J and Chin S 2012 Photocatalytic degradation of methylene blue by a combination of TiO_2-anatase and coconut shell activated carbon *Powder Technol.* **225** 167–75
[3] Tayade R J, Kulkarni R G and Raksh. V 2006 Jasra. Transition metal ion impregnated mesoporous TiO_2 for photocatalytic degradation of organic contaminants in water *Ind. Eng. Chem. Res.* **45** 5231–8
[4] Nigam P, Armour G, Banat I, Singh D and Marchant R 2000 Physical removal of textile dyes from effluents and solid-state fermentation of dye-adsorbed agricultural residues *Bioresoure Technol.* **72** 219–26
[5] Murugan K, Rao T N, Gandhi A S and Murty B 2010 Effect of aggregation of methylene blue dye on TiO_2 surface in self-cleaning studies *Catal Commun.* **11** 518–21
[6] Kapdan I K and Kargi F 2002 Simultaneous biodegradation and adsorption of textile dyestuff in an activated sludge unit *Process Biochem.* **37** 973–81
[7] Schäfer A, Nghiem L and Waite T 2003 Removal of the natural hormone estrone from aqueous solutions using nanofiltration and reverse osmosis *Environ. Sci. Technol.* **37** 182–8
[8] Arslan I, Balcioğlu I A and Bahnemann D W 2000 Advanced chemical oxidation of reactive dyes in simulated dyehouse effluents by ferrioxalate-Fenton/UV-A and TiO_2/ UV-A processes *Dyes Pigm.* **47** 207–18
[9] Van der Zee F P and Villaverde S 2005 Combined anaerobic-aerobic treatment of azo dyes-A short review of bioreactor studies *Water Res.* **39** 1425–40
[10] Zhang M, Wang J and Fu H 2008 Preparation and photocatalytic activity of nanocrystalline TiO_2 with uniform shape and size *J. Mater. Process. Technol.* **199** 274–8
[11] Giwa A, Nkeonye P, Bello K, Kolawole E and Campos A 2012 Solar photocatalytic degradation of reactive yellow 81 and reactive violet 1 in aqueous solution containing semiconductor oxides *Int. J. Appl. Sci. Tech.* **2** 90–105
[12] Liu K, Zhu L, Jiang T, Sun Y, Li H and Wang D 2012 Mesoporous TiO_2 micro-nanometer composite structure: synthesis, optoelectric properties, and photocatalytic selectivity *Int. J. Photoenergy* **2012** 1–9
[13] Petronella F *et al* 2017 Colloidal nanocrystalline semiconductor materials as photocatalysts for environmental protection of architectural stone *Crystals.* **7** 30
[14] Jain R and Sikarwar S 2008 Photodestruction and COD removal of toxic dye erioglaucine by TiO_2-UV process: influence of operational parameters *Int. J. Phys. Sci.* **3** 299–305
[15] Wu C H and Chern J M 2006 Kinetics of photocatalytic decomposition of methylene blue *Ind. Eng. Chem. Res.* **45** 6450–7
[16] Hoffmann M R, Martin S T, Choi W and Bahnemann D W 1995 Environmental applications of semiconductor photocatalysis *Chem. Rev.* **95** 69–96
[17] Ghanbarian M, Nabizadeh R, Mahvi A, Nasseri S and Naddafi K 2011 Photocatalytic degradation of linear alkyl benzene solfunate from aqueous solution by TiO_2 nanoparticles *Iran J. Environ. Health Sci. Eng* **8** 309–16
[18] Lakshmi S, Renganathan R and Fujita S 1995 Study on TiO_2-mediated photocatalytic degradation of methylene blue *J Photochem Photobiol,* A **88** 163–7
[19] Liu J, An T, Li G, Bao N, Sheng G and Fu J 2009 Preparation and characterization of highly active mesoporous TiO_2 photocatalysts by hydrothermal synthesis under weak acid conditions *Microporous Mesoporous Mater.* **124** 197–203
[20] Yu J, Liu S and Yu H 2007 Microstructures and photoactivity of mesoporous anatase hollow microspheres fabricated by fluoride-mediated self-transformation *J. Catal.* **249** 59–66
[21] Fan X, Yu T, Zhang L, Chen X and Zou Z 2007 Photocatalytic degradation of acetaldehyde on mesoporous TiO_2: effects of surface area and crystallinity on the photocatalytic activity *Chin. J. Chem. Phys.* **20** 733–8
[22] Lin X, Rong F, Ji X and Fu D 2011 Carbon-doped mesoporous TiO_2 film and its photocatalytic activity *Microporous Mesoporous Mater.* **142** 276–81
[23] Fu G, Vary P S and Lin C T 2005 Anatase TiO_2 nanocomposites for antimicrobial coatings *J. Phys. Chem.* B **109** 8889–98
[24] Mohammad H H J, Al-Asfoor F, Radiman S and Umar A A 2012 Dressing of MWCNTs with TiO_2 nanoparticles using modified microwave method *Adv Mater Res.* **364** 228–31
[25] Song C *et al* 2009 Efficient fabrication and photocatalytic properties of TiO_2 hollow spheres *Catalysis Commun.* **10** 650–4

[26] Sungmin C, Eunseuk P, Minsu K and Jongsoo J 2010 Photocatalytic degradation of methylene blue with TiO_2 nanoparticles prepared by a thermal decomposition process *Pow Tech.* **201** 171–6
[27] Chin S, Park E, Kim M, Jeong J, Bae G N and Jurng J 2011 Preparation of TiO_2 ultrafine nanopowder with large surface area and its photocatalytic activity for gaseous nitrogen oxides *Powder Technol.* **206** 306–11
[28] Yu J, Liu W and Yu H 2008 A one-pot approach to hierarchically nanoporous titania hollow microspheres with high photocatalytic activity *Crystal Growth and Design* **8** 930–4
[29] Kondo Y *et al* 2008 Preparation, photocatalytic activities, and dye-sensitized solar-cell performance of submicron-scale TiO_2 hollow spheres *Langmuir* **24** 547–50
[30] Baharvand A, Ali R, Yusof A M, Ibrahim A N, Chandren S and Nur H 2014 Preparation of anatase hollow TiO_2 spheres and their photocatalytic activity in the photodegradation of chlorpyrifos *J. Chinese Chem. Soc.* **61** 1211–6
[31] Dwivedi C, Dutta V, Chandiran A K, Nazeeruddin M K and Grätzel M 2013 Anatase TiO_2 hollow microspheres fabricated by continuous spray pyrolysis as a scattering layer in dye-sensitised solar cells *Energy Procedia.* **33** 223–7
[32] Qu X, Yan X, Hou Y, Wang P, Song H and Du F 2015 Preparation of Gd-doped TiO_2 hollow spheres with enhanced photocatalytic performance *J. Sol-Gel Sci. Technol.* 1–9
[33] Murugan A V, Samuel V and Ravi V 2006 Synthesis of nanocrystalline anatase TiO_2 by microwave hydrothermal method *Mater. Lett.* **60** 479–80
[34] Ridha N J, Umar A A, Alosfur F, Jumali M H H and Salleh M M 2013 Microwave assisted hydrothermal method for porous zinc oxide nanostructured-films *J. Nanosci. Nanotechnol.* **13** 2667–74
[35] Yu J and Shi L 2010 One-pot hydrothermal synthesis and enhanced photocatalytic activity of trifluoroacetic acid modified TiO_2 hollow microspheres *J. Molecular Catalysis A: Chemical* **326** 8–14
[36] Huang C-H, Yang Y-T and Doong R-A 2011 Microwave-assisted hydrothermal synthesis of mesoporous anatase TiO_2 via sol–gel process for dye-sensitized solar cells *Microporous Mesoporous Mater.* **142** 473–80
[37] Li J *et al* 2012 Electrospinning synthesis and photocatalytic activity of mesoporous TiO_2 nanofibers *Scientific World J.* **2012** 1–7
[38] Yu J, Wang G, Cheng B and Zhou M 2007 Effects of hydrothermal temperature and time on the photocatalytic activity and microstructures of bimodal mesoporous TiO_2 powders *Appl. Catalysis* B **69** 171–80
[39] Lin Y-T, Weng C-H and Tzeng T W 2010 Photocatalysis and catalytic properties of nano-sized N-TiO_2 catalyst synthesized by sol–gel methods *J. Advanced Oxidation Tech.* **13** 297–304
[40] Weidler P G 1997 BET sample pretreatment of synthetic ferrihydrite and its influence on the determination of surface area and porosity *J. Porous Mater.* **4** 165–9
[41] Lowell S and Shields J E 1991 *Powder Surface Area and Porosity* (London: Chapman & Hall)
[42] Han S *et al* 2005 Low-temperature synthesis of highly crystalline TiO_2 nanocrystals and their application to photocatalysis *Small* **1** 812–6
[43] Bakardjieva S *et al* 2006 Transformation of brookite-type TiO_2 nanocrystals to rutile: correlation between microstructure and photoactivity *J. Mater. Chem.* **16** 1709–16
[44] Huang W, Tang X, Wang Y, Koltypin Y and Gedanken A 2000 Selective synthesis of anatase and rutile via ultrasound irradiation *Chem Commun.* 1415–6
[45] Yu J C, Yu J, Zhang L and Ho W 2002 Enhancing effects of water content and ultrasonic irradiation on the photocatalytic activity of nano-sized TiO_2 powders *J. Photochem. Photobiol.* **148** 263–71
[46] Ye M, Chen Z, Wang W, Shen J and Ma J 2010 Hydrothermal synthesis of TiO_2 hollow microspheres for the photocatalytic degradation of 4-chloronitrobenzene *J. Hazardous Mater.* **184** 612–9
[47] Zhang F, Zhang Y, Song S and Zhang H 2011 Superior electrode performance of mesoporous hollow TiO_2 microspheres through efficient hierarchical nanostructures *J. Power Sources* **196** 8618–24
[48] Deng D, Kim M G, Lee J Y and Cho J 2009 Green energy storage materials: nanostructured TiO_2 and Sn-based anodes for lithium-ion batteries *Energy Env. Sci.* **2** 818–37
[49] Kim D S and Kwak S-Y 2007 The hydrothermal synthesis of mesoporous TiO_2 with high crystallinity, thermal stability, large surface area, and enhanced photocatalytic activity *Appl. Catalysis* A **323** 110–8
[50] Yu J and Wang G 2008 Hydrothermal synthesis and photocatalytic activity of mesoporous titania hollow microspheres *J. Phys. Chem. Solids* **69** 1147–51
[51] Yu J, Yu H, Cheng B, Zhou M and Zhao X 2006 Enhanced photocatalytic activity of TiO_2 powder (P25) by hydrothermal treatment *J. Mol. Catalysis* A **253** 112–8
[52] Xiang Q, Lv K and Yu J 2010 Pivotal role of fluorine in enhanced photocatalytic activity of anatase TiO_2 nanosheets with dominant (001) facets for the photocatalytic degradation of acetone in air *Appl. Catalysis* B **96** 557–64
[53] Liu S, Yu J and Jaroniec M 2010 Tunable photocatalytic selectivity of hollow TiO_2 microspheres composed of anatase polyhedra with exposed {001} facets *J. Am. Chem. Soc.* **132** 11914–6
[54] Cho S and Lee K-H 2010 Synthesis of crystalline TiO_2 nanostructure arrays by direct microwave irradiation on a metal substrate *J. Cryst. Growth* **312** 1785–8
[55] Hu C, Duo S, Liu T, Li W and Zhang R 2010 Low temperature facile synthesis of anatase TiO_2 coated multiwalled carbon nanotube nanocomposites *Mater. Lett.* **64** 2472–4
[56] Chun Zeng H 2007 Ostwald ripening: a synthetic approach for hollow nanomaterials *Current Nanoscience.* **3** 177–81
[57] Yao J and Wang C 2010 Decolorization of methylene blue with TiO_2 sol via UV irradiation photocatalytic degradation *Int. J. Photoenergy* **2010** 1–6
[58] Ren T-Z, Yuan Z-Y and Su B-L 2003 Surfactant-assisted preparation of hollow microspheres of mesoporous TiO_2 *Chem. Phys. Lett.* **374** 170–5
[59] Feng X, Yang L and Liu Y 2010 Preparation of titania hollow spheres by catalyst-free hydrothermal method and their high thermal stabilities *Appl. Surf. Sci.* **257** 756–61
[60] Feng X, Yang L and Liu Y 2010 A simple one-step fabrication of micrometer-scale hierarchical TiO_2 hollow spheres *Mater. Lett.* **64** 2688–91
[61] Alosfur F K M, Jumali M H, Radiman S, Ridha N J and Umar A A 2013 Visible light photocatalytic activity of TiO_2/MWCNTs nanocomposite prepared using modified microwave technique *Sensing Technology (ICST), Seventh Int. Conf. on, IEEE2013* pp 777–81
[62] Mukhlish M, Najnin F, Rahman M and Uddin M 2013 Photocatalytic degradation of different dyes using TiO_2 with high surface area: a kinetic study *J. Sci. Research* **5** 301–14